HOKKAIDO UNIVERSITY

Title	Effects of non-equilibrium angle fluctuation on F-1-ATPase kinetics induced by temperature increase
Author(s)	Tamiya, Yuji; Watanabe, Rikiya; Noji, Hiroyuki et al.
Citation	Physical chemistry chemical physics, 20(3), 1872-1880 https://doi.org/10.1039/c7cp06256g
Issue Date	2018-01-21
Doc URL	https://hdl.handle.net/2115/72344
Type	journal article
File Information	YTamiya_F1paper_resubmission_final1206.pdf

Hokkaido University Collection of Scholarly and Academic Papers : HUSCAP

PCCP

ARTICLE TYPE

Cite this: DOI: 10.1039/xxxxxxxxxx

Effects of non-equilibrium angle fluctuation on F_1-ATPase kinetics induced by temperature increase†

Yuji Tamiya,[a,d] Rikiya Watanabe,[b] Hiroyuki Noji,[b] Chun-Biu Li,[c,d] and Tamiki Komatsuzaki[d]

Received Date
Accepted Date

DOI: 10.1039/xxxxxxxxxx

www.rsc.org/journalname

F_1-ATPase (F_1) is an efficient rotary protein motor, whose reactivity is modulated by the rotary angle to utilize the thermal fluctuation. In order to elucidate how its kinetics is affected by the change in the fluctuation, we extend the reaction-diffusion formalism [R. Watanabe *et al., Biophys. J.*, 2013, **105**, 2385] applicable to a wider range of temperature based on experimental data analysis of F_1 derived from thermophilic *Bacillus* at high ATP concentration condition. Our simulation shows that the rotary angle distribution manifests stronger non-equilibrium feature as the temperature increases, because ATP hydrolysis and P_i release are more accelerated compared with the timescale of rotary angle relaxation. This effect causes the rate coefficient obtained from dwell time fitting to deviate from the Arrhenius relation in P_i release, which has been assumed in previous activation thermodynamic quantities estimation using linear Arrhenius fitting. Larger negative correlation is also found between hydrolysis and P_i release waiting time in a catalytic dwell with the increase in temperature. This loss of independence between the two successive reactions at the catalytic dwell sheds doubt on the conventional dwell time fitting to obtain rate coefficients with a double exponential function at temperature higher than 65°C, which is close to the physiological temperature of the thermophilic *Bacillus*.

1 Introduction

F_1-ATPase (F_1) is a rotary protein motor driven by ATP hydrolysis,[1,2] whose minimum component for operation consists of an $(\alpha\beta)_3$ stator ring and a rotary shaft γ penetrating the ring.[3] This catalytic sub-complex of F_oF_1-ATP synthase has three catalytic sites on the $(\alpha\beta)_3$ cylinder, where bounded ATP is hydrolyzed into ADP and inorganic phosphate (P_i), accompanying cooperative conformational changes to induce a counter-clockwise γ-subunit rotation viewed from the membrane side. The prominent feature of this enzyme is the extremely high energy conversion efficiency through its tight chemo-mechanical coupling; precise torque measurement experiments[4,5] revealed that the work done by the γ rotation amounts to the ATP hydrolysis free energy.

In order to unveil the working principle to perform this marvelous property, extensive single molecule studies have been carried out to elucidate the tight coupling between γ rotation and intermediate catalytic reactions on $(\alpha\beta)_3$. Rotary assays with an optical microscope tethering a probe (actin filament, bead or gold nano particle) to the γ-subunit of F_1 derived from thermophilic *Bacillus*, TF_1, show 120° stepwise rotations, at each of which a single ATP is hydrolyzed.[2] These 120° steps are further decomposed into 80° and 40° sub-steps.[6,7] The dwell time for these substeps obeys single or double exponential distributions. By combining analyses with mutants and solution with different ligand concentration, the "rate constants" obtained from directly fitting such dwell time distributions provided keys to reveal the elementary steps and kinetic pathways of the catalytic reactions; the 80° step is triggered by ATP binding and ADP release,[6,8] and the 40° step is by hydrolysis of ATP and P_i release.[7–9] The dwells before the 80° and 40° steps are therefore termed the binding and catalytic dwells, respectively. From the temperature dependence[10] of these dwell time exponents, activation free energies are also obtained by the Arrhenius analysis.[11,12]

On the other hand, stall-and-release experiments with magnetic tweezers show that the rate constants of the catalytic reactions depend on the rotation angle of γ, suggesting that the thermal fluctuations of γ can play important roles in modulating the kinetics.[13,14] For example, a recent study with contemporary

[a] *Department of Mathematics, Hokkaido University, Sapporo 001-0020, Japan.*
[b] *Department of Applied Chemistry, University of Tokyo, Tokyo 113-8656, Japan.*
[c] *Current address: Department of Mathematics, Stockholm University, Stockholm, Sweden; Email: cbli@math.su.se*
[d] *Research Institute for Electronic Science, Hokkaido University, Sapporo 001-0020, Japan; Email: tamiki@es.hokudai.ac.jp*

† Electronic Supplementary Information (ESI) available: See DOI: 10.1039/b000000x/

time series analysis revealed a "key" and "lock" role of ATP hydrolysis to regulate the subsequent P_i release rate through a small rotation during a catalytic dwell,[15] which suggests an intimate dependence between the two reactions at the catalytic dwell intermediated by the γ rotary dynamics. Moreover, for the rate constant of P_i release whose angle sensitivity is the biggest among the other elementary steps, the reaction-diffusion (or potential switching) model[16–18] has succeeded in explaining the friction dependence of the overall rate coefficient obtained from fitting the dwell time distributions combining with single F_1 rotary assay with different probe sizes.[19]

Meanwhile, the reaction-diffusion formalism has been studied to explain anomalous chemical kinetics induced by the protein conformational fluctuation. In theoretical studies, the competition between the diffusion timescale and the reaction timescale brings about non-equilibrium conformational fluctuation, which was expected to lead to non-exponential kinetics[20,21] and non-Arrhenius temperature dependence of the rate coefficient.[22,23] As the development of the single-molecule measurement, the correlation in the catalytic turnover time was also found and explained in the same formalism.[24–27]

In this study, we investigated how the rotary angle fluctuation changes with temperature and affects the kinetics in catalytic dwells of F_1 originated from thermophilic *Bacillus*. Based on the time series analysis of single molecule rotary traces at different temperature,[11] we extended the potential switching model[15,19] so as to be applicable to a wider range of temperature. Through systematical Brownian dynamics simulation, it is found that the higher temperature is, the larger the rotary angle fluctuations deviates from the local-equilibrium distribution in both pre- and post-hydrolysis states due to slower diffusion relative to reaction timescales. For the angle-sensitive P_i release reaction, this non-equilibrium fluctuation brings about non-Arrhenius temperature dependence and our improved thermodynamic analysis result provides positive activation entropy contrary to the previous result based on linear Arrhenius fitting,[11] which is more natural in the view point of protein structures. We also show increasing negative correlation between dwell times of hydrolysis and P_i release in a catalytic dwell with the increase in temperature.

2 Methods and Model

2.1 A Potential Switching Model of Chemo-mechanical Couplings for the F_1 Catalytic Dwell

In order to scrutinize the rotary angle fluctuation and change of kinetics under a wider range of temperature, we adopted a potential switching model.[15,19] The rotary angle θ during a dwell diffuses on a potential, which switches to other potentials stochastically driven by chemical reactions. A schematic of this model is depicted in Fig. 1. Each harmonic potential represents the free energy profile $G(\theta)$ of a single catalytic step that can be resolved at high ATP concentrations, namely, the ATP hydrolysis and P_i-release. Under the free rotation condition, it was recently found that the ATP hydrolysis proceeds before the P_i-release with low synthesis rates.[15] In addition, a small but detectable rotation ($\sim 20^\circ$) triggered by ATP hydrolysis was revealed, which is manifested in the separation of the two potential surfaces of pre- and post-hydrolysis states. After P_i-release, the system leaves the post-hydrolysis surface and the current catalytic dwell ends. It then lands on the pre-hydrolysis state of the next catalytic dwell (see Fig. 1). After the switching, the system undergoes a power stroke where the γ-angle rotates $\sim 100^\circ$ toward the equilibrium position of the pre-hydrolysis state.

While the stochastic potential switchings (reactions) are governed by the rate constants, we model the diffusion of θ_γ on a potential surface by the overdamped Langevin equation;

$$\Gamma \frac{d\theta}{dt} = -\frac{dG^{\mathrm{pre/post}}(\theta)}{d\theta} + \sqrt{2\Gamma k_B T}\,\xi(t), \tag{1}$$

where θ, Γ, k_B, and T correspond to the rotary angle of the γ-subunit, the effective friction constant of the probe bead, the Boltzmann constant, and temperature, respectively. $\xi(t)$ is Gaussian white noise satisfying $\langle \xi(t) \rangle = 0$ and $\langle \xi(0)\xi(t) \rangle = \delta(t)$. $\langle \cdot \rangle$ represents an ensemble average. The free energy potential for the pre- or post-hydrolysis dwell $G^{\mathrm{pre/post}}(\theta)$ is basically a harmonic potential $\kappa(\theta - \theta_0^{\mathrm{pre/post}})^2/2$ but it is smoothly connected to linear ones in the outer region so that the torque $|dG/d\theta|$ should not exceed the experimental value[19,29] (More details are in SI). $\theta_0^{\mathrm{pre/post}}$ represents the equilibrium position of the potential, $\theta_0^{\mathrm{pre}} = -10^\circ$ and $\theta_0^{\mathrm{post}} = +10^\circ$, reflecting a small 20° rotation after hydrolysis recently found.[15] Because the free energy landscape is 120° periodic due to the three fold symmetric structure of the $(\alpha\beta)_3$-subunit, the rotary angle shifts -120° when P_i release happens and the system goes to the next catalytic dwell.

Because the mobility of the γ-subunit rotation is affected by the friction exerted on the rotation probe from the viscous media, the effective friction constant Γ is determined using the fluid mechanics relation $\Gamma = (8\pi a^3 + 6\pi a x_r^2)\eta(T)$,[6] where a, x_r, and $\eta(T)$ are the probe radius, revolution radius of the probe, and the viscosity of the media, respectively. We assumed that the media viscosity has the same temperature(T)-dependence as that of pure water so that the diffusion timescale ($\propto \tau_{\mathrm{rel}} = \Gamma/\kappa$, where κ is the curvature of the quadratic potential) gets shorter with the increase in temperature with almost an exponential form.

The dependence of rate constants of potential switching on the rotary angle[14] signifying the modulation of the catalytic rates by the γ-rotation is the key manifestation of chemo-mechanical coupling in the F_1 kinetics. These angle-dependent rate constants are modeled as follows;

$$k_i(\theta;T) = \nu_i \exp\left\{-\frac{1}{k_B T}(\varepsilon_i - \alpha_i \theta)\right\}, \tag{2}$$

where i indicates either hydrolysis or P_i release, $\theta = 0^\circ$ corresponds to the center angle of the catalytic dwell, ν_i and $(\varepsilon_i, \alpha_i)$ are the prefactor and parameters specifying the angle-dependent activation free energy (more precisely, $(\varepsilon_i - \alpha_i\theta)$ equals to the enthalpy shown later in eq.(6b), respectively. This angle-dependence reflects the results of stall-and-release experiments $k_i(\theta) \propto e^{b_i\theta}$ (i.e., $b_i = \alpha_i/k_BT$) with $b_{\mathrm{hyd}} \sim 0.02$ degree^{-1} and $b_{\mathrm{Pi}} \sim 0.12$ degree^{-1} at room temperature,[13,14] implying a linear angle dependence of the activation free energy barriers. We remark here that the angle dependence is stronger in P_i-release than

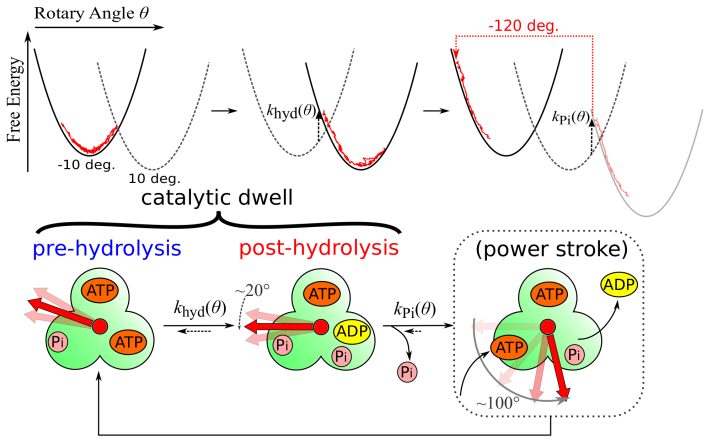


Fig. 1 The kinetic scheme and the potential switching model for the F_1 catalytic dwell. In the lower part the kinetic scheme is described with the schematic picture of F_1 molecules watched from above. The red arrows indicate the rotary angle of the γ-subunit and the green area represents the three catalytic sites of the $(\alpha\beta)_3$-subunit. After ATP hydrolysis on one of the catalytic sites, the inorganic phosphate (P_i) on another site is released and the system moves to the next catalytic state, accompanying large rotation called power stroke. At high ATP concentration, ATP binding and ADP release are too short and neglected. In the upper part the potential switching model of the corresponding states is described. The γ-angle during a catalytic state traps and diffuses on the free energy potentials $G(\theta)$. Each catalytic dwell consists of two harmonic potentials corresponding to the pre- and post-hydrolysis states separated by $\sim 20^\circ$. The system makes transition from one potential to another successively according to the angle-dependent rate constants $k_i(\theta)$.[13,28] Considering the 120° periodicity of the free energy landscape, the system returns to the pre-hydrolysis state with -120° angle shift after P_i release.

in hydrolysis, which suggests that the P_i release contributes more to the torque generation than hydrolysis.[30]

2.2 Experimental Data Analysis for the Parameter Tuning

In order to tune the parameters of the model discussed in the previous subsection, we provided time series analysis to the experimental data and extracted physical quantity so that the model is consistent with reality. The data we analyzed is the same as those in R. Watanabe et al. 2014[11]. The rotation of single wild type F_1 from thermophilic *Bacillus*, TF_1, (physiological temperature at 75°C) was observed with the laser dark-field microscopy[11,31] with time resolution at 27,000 frames per sec (fps) by attaching an 80 nm gold bead as a probe to the γ-subunit. The rotation assay was performed under high ATP concentration ([ATP]=200μM) so that the binding dwell is fast and becomes invisible in the rotary time trace. In this condition, we can focus on catalytic dwells, where the rate of the P_i release step is sensitive to the rotary angle fluctuation. The temperature was set to be 16, 20, 25, 33°C($\pm$0.1°C). Due to the attachment of an F_1 molecule to Ni-NTA coated glass surface via His-tag and heat resistance properties of the camera lens, it is difficult to measure the rotation at temperature higher than 33°C or lower than 10°C.

Among the model parameters, the rate constants parameters ν_i, ε_i can be obtained from the rate coefficients, fitting exponents of the dwell time distribution, at $T = 20, 25, 33^\circ$C and the effective friction Γ from the decay rate of the rotary angle autocorrelation during a catalytic dwell $\langle\theta(0)\theta(t)\rangle$. Further details of the parameter tuning are in SI but we mention here the objective methods to select out catalytic dwells distinctly from the time series and make remarks on the rate coefficients obtained from the free rotation experiments.

Following our previous work,[15] the rotation and pause parts in the time series were selected out by objectively determining where a pause/rotation starts and ends. This was performed using change point analysis that detects the time instants in the rotary traces at which the linear trends of the angle change. We note that the employed change point analysis does not need to assume any noise model of the angular fluctuations. In terms of a clustering method also developed in our previous studies,[15,32] the resulting change point intervals are then classified into three groups corresponding to the three catalytic dwells in one full rotation of the γ-subunit. In our analysis, kinetics from different catalytic dwells of the same molecule are analyzed separately in order to take account of the local heterogeneity around the motor (except for 16°C data, more details are in Appendix).

We next obtained the rate coefficients of ATP hydrolysis and P_i release reactions from the dwell time distribution of the catalytic dwells. As the two reactions take place during each catalytic dwell, the dwell-time survival distribution $S(\tau)$ is fitted with a double exponential function $c_1 \exp(-k_{hyd}\tau) + c_2 \exp(-k_{P_i}\tau)$, where c_1, c_2 are constants, k_{hyd} and k_{P_i} are the "rate constants", which relate to the time constants of the hydrolysis and P_i release reactions by $\tau_{hyd} = 1/k_{hyd}$ and $\tau_{P_i} = 1/k_{P_i}$, respectively. More details of the curve fitting are in Appendix. Although the quantities obtained here have been called "rate constants" conventionally in experiments, we remark that they are different from the angle-dependent rate constants $k_i(\theta)$ revealed by the stall-and-release experiment.[14] While we regard the angle-dependent rate constants as the rate constants in the ordinary sense, the exponents of the dwell time distribution could be understood as the values of $k_i(\theta)$s averaged over the fluctuating rotary angles during the catalytic dwells. In this paper we call these quantities as rate co-

efficients denoted by $\bar{k}_i$ to distinguish from the angle-dependent rate constants.

3 Results and Discussion

3.1 Temperature Dependence of the rate coefficients

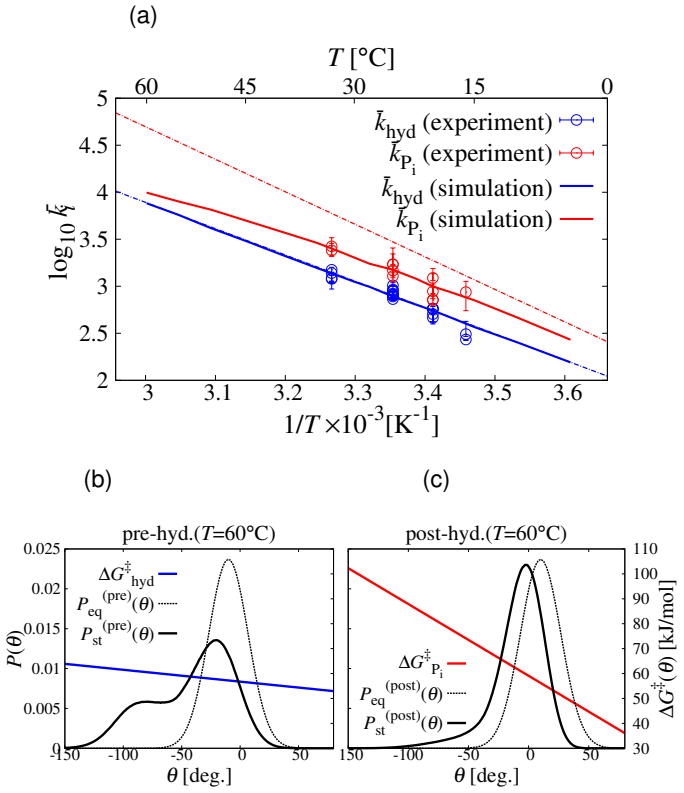


Fig. 2 The Arrhenius plot and the non-equilibrium angle fluctuation. (a) Temperature dependence of the rate coefficients ($1/T$ vs $\log \bar{k}_i$) for hydrolysis (blue) and P_i release (red). Solid line and curve are rate coefficients obtained from the simulation, whereas circles are the experimental values at 16, 20, 25, and 33°C with error bars signifying 68% confidence intervals based on the change point detection uncertainty (see Appendix). Broken lines are hypothetical fast diffusion limit values $\bar{k}_i^{\mathrm{FDL}}$ with the local-equilibrium assumption (eq.(**??**. In order to make a clearer correspondence between rate constants and the angle fluctuation, the steady state γ-angle distributions (solid curves) at 60°C in pre-hydrolysis (b) and post-hydrolysis (c) dwells are shown with (Gibbs') activation free energy $\Delta G_i^{\ddagger}(\theta)$ calculated as eq. (3) (blue and red lines). The broken curves are the local-equilibrium angle distributions, i.e., Boltzmann distributions. The left peak of the stationary angle distribution of the pre-hydrolysis dwell around θ = -100° is an artifact due to the potential cut-off (see SI).

We first explored the temperature dependence of the rate coefficients of hydrolysis and P_i release for a wide range of temperature based on the reaction-diffusion model described in Sec. 2.1.

Fig. 2(a) shows the relationship between inverse temperature $1/T$ and the logarithm of the rate coefficients of hydrolysis and P_i release, $\bar{k}_{\mathrm{hyd}}$ and $\bar{k}_{P_i}$, where straight lines in the plot indicate Arrhenius relations. While hydrolysis (blue solid line) appears to obey the Arrhenius relation, the slope of the rate coefficient of P_i-release (red solid curve) gets less steep as the temperature rises. This is caused by a combining effects of the strong angle sensitivity of its rate constant $k_{P_i}(\theta)$ and the non-equilibrium angle fluctuation as follows.

As shown in Fig. 2(c), at the high temperature regime $\sim 60^{\circ}$C in the post-hydrolysis potential, the steady state distribution of the rotary angle $P_{\mathrm{st}}^{\mathrm{post}}(\theta)$ (black solid curve) deviates from the local-equilibrium distribution $P_{\mathrm{post}}^{\mathrm{eq}}(\theta) \propto \exp\{-G^{\mathrm{post}}(\theta)/k_BT\}$ (black broken curve). The red line in the figure is the activation free energy of the reaction, which was calculated from the angle-dependent rate constant as

$$\Delta G_i^{\ddagger}(\theta) = -k_BT \log\left(\frac{hk_i(\theta)}{k_BT}\right) \tag{3}$$

based on the transition state theory[33,34] (see also the section 3.2). This implies that the γ angle tends to be more populated in the smaller angle region, where the activation free energy is higher due to the strong angle dependence. Although the activation free energy does not change so much with temperature, the steady state angle distribution shifts toward the smaller angle region as the temperature increases (see its temperature dependence in SI). This mechanism suppresses the linear acceleration of the rate coefficient of P_i-release as the temperature increases. As a guide to show this mechanism, we also calculated the hypothetical rate constants assuming local-equilibrium angle distribution in each potential, that is, the fast diffusion limit (FDL),

$$\bar{k}_i^{\mathrm{FDL}}(T) = \int k_i(\theta;T) P_{\mathrm{pre/post}}^{\mathrm{eq.}}(\theta;T) d\theta \tag{4}$$

(broken lines in Fig. 2(a)). For the P_i release, the simulation value of $\bar{k}_{P_i}$ deviates more from the FDL (red broken line) as the temperature increases, suggesting that the system is further from equilibrium at higher temperature.

On the other hand in hydrolysis, the simulation line (blue solid line) coincides with the FDL (blue broken line) in Fig. 2(a). It should be noted however that in Fig. 2(b) the stationary angle distribution shows a stronger non-equilibrium feature than in P_i release (see also its temperature dependence in SI). This is explained by the weak angle dependence of the hydrolysis activation energy (blue line in Fig. 2(b)). Because the dwell time in the pre-hydrolysis potential is less affected by the angle fluctuation during the dwell, the hydrolysis rate coefficient $\bar{k}_{\mathrm{hyd}}$ is not different from that of FDL regardless of how far the angle fluctuation deviates from local-equilibrium.

The cause of these non-equilibrium angle distributions is the competition between two timescales;[20,21] the diffusion timescale and the reaction timescales. When the system lands on a pre- or post-hydrolysis dwell, it thermally diffuses over the potential and relaxes towards local-equilibrium, losing the mechanical memory. If this diffusion timescale is fast enough compared with that of the chemical reaction, i.e., hydrolysis or P_i release, the reaction brings the system to the next potential after the local-equilibration, establishing the quasi-equilibrium state. On the other hand, when the reaction and diffusion timescales are comparable, the system moves to the next potential before the local-equilibration is completed, resulting in a non-equilibrium angle distribution. In our system, both the diffusion and the reactions get faster at higher temperature; the former due to lower viscosity of the media and the latter due to the Arrhenius relation assumed for each fixed

rotary angle. In particular, our model with parameters inferred from the single molecule rotary data indicates that the reactions outrun the diffusion as the temperature gets higher, say, equal to or larger than 60 $\sim$ 70°C, bringing the system to a more non-equilibrium state.

3.2 Thermodynamic Analysis with Non-Arrhenius Modification

Table 1 Comparison of thermodynamic quantities for reactions at 25°C

units: [kJ/mol]		$\Delta G_i^\ddagger$	$\Delta H_i^\ddagger$	$T\Delta S_i^\ddagger$
Watanabe et al. 2014[11]	Hydrolysis	56	51	-5.4
	P_i release	53	39	-14
Non-Arrhenius modification	Hydrolysis	57	54	-2.9
	P_i release	55	68	13

In the previous work,[11] the transition state thermodynamic quantities, that is, the activation Gibbs free energy ($\Delta G^\ddagger$), enthalpy ($\Delta H^\ddagger$), and entropy ($T\Delta S^\ddagger$), were obtained by linear fitting of the Arrhenius plot for the rate coefficients $\bar{k}_{\rm hyd}$ and $\bar{k}_{\rm P_i}$ from the same range of temperature in this work. The Arrhenius relation $\bar{k}_i \propto \exp(-\Delta G_i^\ddagger/k_BT)$ was assumed to hold for all temperature in the previous study. From the thermodynamic relation $\Delta G_i^\ddagger = \Delta H_i^\ddagger - T\Delta S_i^\ddagger$, the slope of the fitting corresponds to $\Delta H_i^\ddagger$ and that the intercept with the y-axis at $T \to \infty$ corresponds to $\Delta S_i^\ddagger$. However, the non-Arrhenius relation shown in Fig. 2(a) suggests that the linear fitting estimation may lead to inappropriate values of $\Delta H_i^\ddagger$ and $T\Delta S_i^\ddagger$ because the effective activation free energy barrier height also changes with temperature due to the friction effects on the γ-angle fluctuation. In order to take the effects of nonequilibrium γ-angle fluctuation into account, we recalculated the thermodynamic quantities from the experimentally inferred angle-dependent rate constants eq.(2) used in our model. Comparing them with the thermodynamic representation of the transition state theory[35]

$$k = \frac{k_BT}{h}\exp\left(-\frac{\Delta G^\ddagger}{k_BT}\right) = \frac{k_BT}{h}\exp\left(\frac{\Delta S^\ddagger}{k_B}\right)\exp\left(-\frac{\Delta H^\ddagger}{k_BT}\right), \quad (5)$$

we defined the activation entropy and enthalpy as below, combined with eq.(2);

$$\Delta S_i^\ddagger = k_B \log\left(\frac{h\nu_i}{k_BT}\right) \quad (6a)$$

$$\Delta H_i^\ddagger(\theta) = \varepsilon_i - \alpha_i\theta. \quad (6b)$$

We remark here that the temperature dependence of the prefactor $\nu_i = \frac{k_BT}{h}\exp(\Delta S_i^\ddagger/k_B)$ is so weak that the dominant part of the temperature dependence of the angle-dependent rate constants comes from the exponential term related to the enthalpy.

The results are shown on Table 1, together with the previous results. While $\Delta G_i^\ddagger$ was calculated from the rate coefficient via $-k_BT\log(h\bar{k}_i/k_BT)$, $T\Delta S^\ddagger$ and $\Delta H^\ddagger$ were estimated using the prefactor ν_i (eq.(6a)) and the relation $\Delta H_i^\ddagger = \Delta G_i^\ddagger - T\Delta S_i^\ddagger$, respectively. $\Delta G_i^\ddagger$ and $\Delta H_i^\ddagger$ roughly correspond to the ensemble averages of the angle-dependent values (eq. (3), (6b)) over the rotary angle fluctuation. In the previous linear fitting estimation,[11] both for hydrolysis and P_i release the contribution to the activation free energy from the entropy term was negative. In our recalculation, however, while the hydrolysis shows almost no qualitative change, positive entropy change was found at P_i release. This result is more natural considering that one of the catalytic interfaces opens during a catalytic dwell to release P_i[36] although in the previous study the negative entropy change of P_i release was ascribed to the loss of water entropy due to the loosening of subunit packing.[11,37]

In this study, we assumed no angle dependence in the prefactor ν_i for the sake of the simplicity, which means that the entropy difference between the reactant and the transition state is constant along the γ-subunit rotation (see eq.(6a)). If the activation entropy depends on θ, the angle dependence of the parameter b in the rate constant $k(\theta) \propto e^{b\theta}$ can be represented from the relation (5) as below;

$$b = \frac{d\log k_i(\theta)}{d\theta} = \frac{1}{k_B}\frac{d\Delta S^\ddagger}{d\theta} - \frac{1}{k_BT}\frac{d\Delta H^\ddagger}{d\theta}. \quad (7)$$

In order to elucidate the rotary angle dependence of the entropy contribution $\Delta S_i^\ddagger(\theta)$ from the temperature dependence of b, precise studies with stall-and-release experiments at different temperature are required.[12]

3.3 Correlation between Hydrolysis and P_i Release Waiting Time at High Temperature

The non-equilibrium features observed in Fig. 2 suggest that the memory during a dwell is not completely erased before the potential switching and carried into the next dwell, which may produce correlation between waiting time in successive dwells.

In Fig. 3(a) are shown two types of correlation coefficients (in the sense of Pearson); the one between successive pre- and post-hydrolysis dwell time (blue line) and the other between post-hydrolysis dwell time and the next pre-hydrolysis dwell time (red line). Both are at temperature ranging from 4 to 70°C.

To begin, let us look at the correlation between pre-hydrolysis dwell time ($\tau_{\rm pre}$) and the next post-hydrolysis dwell time ($\tau_{\rm post}$) (blue line): The correlation coefficient becomes more negative as the temperature increases. A negative correlation coefficient means that on average, if hydrolysis takes longer time, the following P_i release takes shorter time, and vise versa. This implies, especially at the high temperature region, that the sum of pre- and post-hydrolysis dwell time, i.e., the total catalytic dwell time, cannot be too long or too short relative to the average value. Actually, the 2D plots for $C(\tau_{\rm pre},\tau_{\rm post}) = P(\tau_{\rm pre},\tau_{\rm post}) - P(\tau_{\rm pre})P(\tau_{\rm post})$ between the dwell time $\tau_{\rm pre}$ and $\tau_{\rm post}$ in Fig. 3 (b)-(d) show that it gets negative when both $\tau_{\rm pre}$ and $\tau_{\rm post}$ are shorter (and longer) as temperature increases from 4°C $\to$ 33°C $\to$ 70°C. As $C(\tau_{\rm pre},\tau_{\rm post}) < 0$ implies $P(\tau_{\rm pre}|\tau_{\rm post}) < P(\tau_{\rm pre})$ and $P(\tau_{\rm post}|\tau_{\rm pre}) < P(\tau_{\rm post})$, this means that at the blue regions the occurrence of $\tau_{\rm pre}$ ($\tau_{\rm post}$) conditioned on $\tau_{\rm post}$ ($\tau_{\rm pre}$) is rarer than the marginal probability $P(\tau_{\rm pre})$ ($P(\tau_{\rm post})$) (see also the relationship between Pearson correlation and two-body correlation in SI).

The essential point to produce this negative correlation is again the angle sensitivity of the rate constant for P_i release. Because P_i

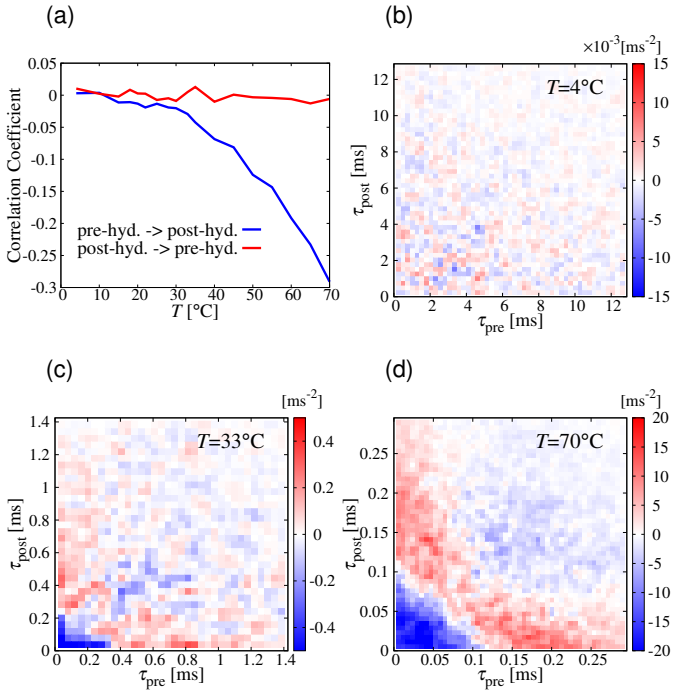


Fig. 3 Temperature dependence of the correlation between pre- and post-hydrolysis dwell time (τ_{pre} and τ_{post}, respectively). (a) The Pearson correlation coefficient for τ_{pre} and τ_{post} during a catalytic dwell (blue line) and the one for τ_{post} and τ_{pre} in the successive catalytic dwells separated by a power stroke (red line). (b)-(d) 2D plots of $C(\tau_{pre},\tau_{post}) = P(\tau_{pre},\tau_{post}) - P(\tau_{pre})P(\tau_{post})$ between the two dwell time during a catalytic dwell at 4°C (b), 33°C (c), 70°C (d). The negative (positive) correlation region is colored with blue (red). The relationship between Pearson correlation coefficient and the joint probabilities is presented in SI.

is more easily released when the γ angle is larger (around 20° in Fig. 2(c)), the post-hydrolysis dwell time τ_{post} strongly depends on how long the γ angle diffused on the pre-hydrolysis potential and at which angle hydrolysis took place to land onto the next post-hydrolysis potential well. When the pre-hydrolysis dwell was long enough for the system to diffuse and approach toward the large θ region before hydrolysis takes place, the subsequent P_i release may not take so long because θ is already close to the region with low activation barrier. However, if the bounded ATP was rapidly hydrolyzed before the γ-subunit could diffuse much toward the large θ region, the system has to take longer time to diffuse into larger θ region in the post-hydrolysis potential where P_i is easily released. Especially hydrolysis tends to take place at smaller angle region with the increase in temperature because the steady-state angle distribution shifts more to the left and $\Delta G^{\ddagger}$ is only weakly dependent on θ (see Fig. 2(b)), which results in the larger negative correlation.

This negative correlation can contribute to generation of a multi-exponential dwell time distribution. Quite often dwell time fitting was employed based on kinetic schemes with independent reaction steps. In particular, dwell time histograms of the catalytic dwell were fitted in recent studies[11,19] with double exponential (probability density) functions of the form $P(\tau) = c(\exp(-k_{hyd}\tau) - \exp(-k_{P_i}\tau))$ with a constant c, which is valid only if the hydrolysis and P_i release reactions are successive and independent. Actually, as the correlation between these two reactions gets larger, the deviation of the dwell time distribution from a double exponential form becomes significant (see also SI). Especially at temperature higher than 65°C, we cannot fit the dwell time distributions properly any more due to the increasing multi-exponentiality. We therefore did not include their rate coefficients from our simulation in the Arrhenius plot (Fig. 2(a)). Moreover, the appearance of multi(>2)-exponential at the catalytic dwell can further be enhanced by the non-equilibrium angle fluctuations in which multiple transition paths can take place,[20,21] each with different reaction timescales due to the strong angle-dependent activation energy especially for the P_i release reaction.

On the contrary, no correlation is detected between post-hydrolysis dwell time and the pre-hydrolysis dwell time of the next catalytic dwell at any temperature investigated (red line in Fig. 3 (a), see also the corresponding 2D plots at three different temperature in SI). This memory loss separated by a power stroke arises from the weak angle dependence of the hydrolysis rate constant, because the pre-hydrolysis dwell time is not affected by the initial distribution of the dwell angle.

4 Conclusion

Using a potential switching model with parameters inferred directly from single F_1 rotary assay to describe the chemo-mechanical coupling of the γ-angle fluctuation and chemical reactions (ATP hydrolysis and P_i release), we have investigated the effects of the rotary fluctuation on the chemical kinetics of the catalytic dwell, especially at temperature higher or lower than room temperature, which experiments cannot currently cover.

We found that the non-equilibrium angle fluctuation induced by the competition between the rotary diffusion timescale and the reaction timescale brings about the non-Arrhenius temperature dependence in the P_i release rate coefficient due to its strong angle sensitivity. While the breakdown of the Arrhenius kinetics had been ascribed to the fluctuation of the activation free energy and the enzyme conformation,[38,39] there were not so extensive discussions on the molecular origin of the fluctuation. Our result showed that the coupling of the diffusive non-equilibrium property caused by the timescales competition and the continuous set of the parallel reaction pathways along with the conformational fluctuation could be the key factor to affect the kinetics. At the same time, the activation entropies and enthalpies estimated previously from experimental data based on Arrhenius relations were generalized to the non-Arrhenius case and their modified values were obtained by the angle-dependent rate constants instead of the rate coefficients directly obtained by dwell time analysis.

In addition, we also showed that the memory of the angle fluctuation during pre-hydrolysis dwell is brought into the post-hydrolysis dwell in non-equilibrium situation and induces correlation between hydrolysis and P_i release reactions. While the correlation reported in catalytic turnover time was positive in preceding studies,[24,26,27] our result for combination of two different chemical reactions showed negative correlation. Although the formerly detected correlation could be due to artifacts in the analysis of the lower S/N ratio data,[40] we hope that it will

be distinctly measured in experiments with F_1-ATPase when the single molecule measurement becomes available at temperature higher than 40°C. We also consider that this negative correlation contributes to the deviation of catalytic dwell time distributions from double exponential functions around $T = 60 \sim 70^\circ$, close to the physiological temperature for the thermophilic *Bacillus*, from which the experimental samples were derived from. In this sense from experimental view points, our result would propose a caution against conventional dwell time analysis in the future, too.

Finally, we remark that the diffusive non-equilibrium effects originated from the inseparability of the diffusion and reaction timescales could also emerge in high friction settings (such as by using larger beads), leading to the appearance of the correlation between P_i release and hydrolysis dwell time and multiple exponentials in the dwell time distributions even at room temperature. This can hold true for other protein systems when some slower degrees of freedom are involved in chemical reactions and we have to take care of the validity of Arrhenius fitting and the ordinary dwell time analysis.

5 Acknowledgment

We acknowledge H. Ueno, H. Teramoto, S. Ito, J. N. Taylor, S. Tsugawa, and S. Sattari for many discussions. This work was partially supported by JSPS, Grant-in-Aid for Scientific Research (No. 25287105) (to T.K.), Grant-in-Aid for Exploratory Research (No. 25650044) (to T.K.), Grant-in-Aid for Scientific Research on Innovative Areas Spying minority in biological phenomena, MEXT (No. 23115007) (to T.K.), Grant-in-Aid for Scientific Research (No. 16H04771) (to. C.B.L.).

Appendix

Data Selection Criteria

The rotary trace on *x-y* plane was first checked to observe the clean circular rotation. If the rotation was heavily distorted, we did not use that data for analysis because it can contain some artifacts, i.e., undesirable interaction with the glass surface or defects in molecules.

In addition, some data showed dwell time distribution with strange statistics such as having an additional small exponent at much longer timescale than hydrolysis and P_i release. We also excluded that kind of data because it can highly affect the data analysis results.

Objective Methods for Dwell Detection and Assignment

In making a dwell time distribution from the experimental data of rotation angle time series, we have to separate dwells and rotations. We first detected time instants where a linear trend drastically changes to find where dwells or rotations begin and end by employing the same change point analysis as in Ref.[15]. The method we used is based on linear fitting with the least square method. We first calculated CUSUM, cumulative sum of the difference between the time series and its linear trend, and regarded the total size of its fluctuation D_{CUSUM} as a criteria to decide whether there is at least one change point or not. Next, we prepared many sets of the difference time series with permuted time ordering and constructed the distribution of D_{CUSUM} from the ensemble of traces with no change point. If D_{CUSUM} of original data is larger than the 95% confident area of that distribution, we declare the existence of change point(s). When the existence of a change point was affirmed, we next detected the location of the point. We divided the time series into two segments at an arbitrary time position and linearly fitted both of the segments separately. The change point we determined is the dividing position where the total error of the fittings was smallest. After that we repeated this procedure to the new segments until no change point can be detected. Uncertainties of the change point positions are also estimated by a bootstrapping method because the error in dwell lengths directly affects the estimation of rate coefficients.

Change point intervals detected above were classified into dwells and rotations. Considering local environment effects, we did not mix up all dwells from the same molecule but assigned each dwell into a pause on one of the three different catalytic sites on the $(\alpha\beta)_3$ stator ring.

The classification method is a soft clustering method based on information theory detailed in Ref.[32] using conditional probabilities for a given detected change point interval to belong to each of the three catalytic dwells. We determined the most optimized clustering with rate distortion theory[41] so that the internal distance among each cluster is minimized while we compressed the data as much as possible. While we evaluated the internal distance between clustered angles in the same cluster by the averaged value of the rotary angle for each change point interval, as a criterion for the data compressibility we calculated the mutual information between time series data before and after the clustering, where the lower this value is the more coarse-grained the clustered data set is.[15]

Further mathematical details of the data processing methods are described in SI of the previous paper[15].

Curve Fitting Methods

The Padé-Laplace method[15,42,43] was applied in dwell time distribution fitting in order to obtain the rate coefficients $\bar{k}_{\mathrm{hyd/P_i}}$ of ATP hydrolysis and P_i release. In this method we first applied Laplace transformation to the survival distribution and found its poles by Padé approximation. Contrary to the ordinary least square fitting method, it evaluates the total form of the fitting function so that it does not underestimate the effect of the tail part with low probability.

In applying this method, we did not *a priori* assume the number of exponents but truncated exponents whose coefficients were negligibly small. As a result, within the range of $T = 4 \sim 60^\circ$C the fitting was best with two exponents for both experimental and simulation data.

Although the middle to the longer timescale of the survival distribution could be well fitted by this method, sometimes it showed slight deviation at the shorter timescale region, which corresponds to the P_i release timescale. In this case, we fitted the residue from an exponential function with the longer time constant by the least squares method to obtain a better fitting and the more accurate rate constant. If this exponent was drastically

deviated from the one from Padé-Laplace method, we did not use this rate constant at further analysis.

Basically, we treated three sets of catalytic dwells, each corresponding to the three different catalytic cites in a molecule, separately to take the local environment difference into account. Among them, we used the set containing more than 100 dwells for statistical analysis at temperature higher than 20°C. However, for the 16°C data, the length of each dwell was longer and hence we could not obtain enough sample number of dwells at each set. In order to increase the number of dwells and construct a dwell time distribution usable for analysis, we merged some of the dwell data sets in the same molecule whose dwell time distributions were judged to be statistically the same with each other based on the Kolmogorov-Smirnov test with 5% significance level.

References

1 H. Noji, R. Yasuda, M. Yoshida and K. Kinosita, *Nature*, 1997, **386**, 299–302.

2 R. Yasuda, H. Noji, K. Kinosita and M. Yoshida, *Cell*, 1998, **93**, 1117–1124.

3 J. P. Abrahams, A. G. W. Leslie, R. Lutter and John E. Walker, *Nature*, 1994, **370**, 621–628.

4 S. Toyabe, T. Okamoto, T. Watanabe-Nakayama, H. Taketani, S. Kudo and E. Muneyuki, *Physical Review Letters*, 2010, **104**, 198103.

5 E.-i. Saita, T. Suzuki, K. Kinosita and M. Yoshida, *Proceedings of the National Academy of Sciences*, 2015, 201422885.

6 R. Yasuda, H. Noji, M. Yoshida, K. Kinosita and H. Itoh, *Nature*, 2001, **410**, 898–904.

7 K. Shimabukuro, R. Yasuda, E. Muneyuki, K. Y. Hara, K. Kinosita and M. Yoshida, *Proceedings of the National Academy of Sciences of the United States of America*, 2003, **100**, 14731–14736.

8 K. Adachi, K. Oiwa, T. Nishizaka, S. Furuike, H. Noji, H. Itoh, M. Yoshida and K. Kinosita, *Cell*, 2007, **130**, 309–321.

9 T. Nishizaka, K. Oiwa, H. Noji, S. Kimura, E. Muneyuki, M. Yoshida and K. Kinosita, *Nature structural & molecular biology*, 2004, **11**, 142–148.

10 S. Furuike, K. Adachi, N. Sakaki, R. Shimo-Kon, H. Itoh, E. Muneyuki, M. Yoshida and K. Kinosita, *Biophysical journal*, 2008, **95**, 761–770.

11 R. Watanabe, Y. Minagawa and H. Noji, *Protein Science*, 2014, **23**, 1773–1779.

12 R. Watanabe and H. Noji, *Scientific Reports*, 2014, **4**, 4962.

13 R. Watanabe, R. Iino and H. Noji, *Nature chemical biology*, 2010, **6**, 814–820.

14 R. Watanabe, D. Okuno, S. Sakakihara, K. Shimabukuro, R. Iino, M. Yoshida and H. Noji, *Nature Chemical Biology*, 2011, **8**, 86–92.

15 C.-B. Li, H. Ueno, R. Watanabe, H. Noji and T. Komatsuzaki, *Nature Communications*, 2015, **6**, 10223.

16 H. Wang, *Journal of Computational and Theoretical Nanoscience*, 2008, **5**, 2311–2345.

17 S. Toyabe, H. Ueno and E. Muneyuki, *EPL (Europhysics Letters)*, 2012, **97**, 40004.

18 K. Kawaguchi, S. I. Sasa and T. Sagawa, *Biophysical Journal*, 2014, **106**, 2450–2457.

19 R. Watanabe, K. Hayashi, H. Ueno and H. Noji, *Biophysical Journal*, 2013, **105**, 2385–2391.

20 N. Agmon and J. Hopfield, *The Journal of Chemical Physics*, 1983, **78**, 6947–6959.

21 R. Zwanzig, *Accounts of Chemical Research*, 1990, **23**, 148–152.

22 N. Agmon and J. J. Hopfield, *The Journal of Chemical Physics*, 1983, **79**, 2042–2053.

23 M. Karplus, *Journal of Physical Chemistry B*, 2000, **104**, 11–27.

24 H. P. Lu, L. Xun and X. S. Xie, *Science (New York, N.Y.)*, 1998, **282**, 1877–1882.

25 G. K. Schenter, H. P. Lu and X. S. Xie, *The Journal of Physical Chemistry A*, 1999, **103**, 10477–10488.

26 A. M. van Oijen, P. C. Blainey, D. J. Crampton, C. C. Richardson, T. Ellenberger and X. S. Xie, *Science (New York, N.Y.)*, 2003, **301**, 1235–1238.

27 B. P. English, W. Min, A. M. van Oijen, K. T. Lee, G. Luo, H. Sun, B. J. Cherayil, S. C. Kou and X. S. Xie, *Nature Chemical Biology*, 2006, **2**, 87–94.

28 R. Watanabe, D. Okuno, S. Sakakihara, K. Shimabukuro, R. Iino, M. Yoshida and H. Noji, *Nature Chemical Biology*, 2011, **8**, 86–92.

29 K. Hayashi, H. Ueno, R. Iino and H. Noji, *Physical Review Letters*, 2010, **104**, 218103.

30 R. Watanabe and H. Noji, *FEBS Letters*, 2013, **587**, 1030–1035.

31 H. Ueno, S. Nishikawa, R. Iino, K. V. Tabata, S. Sakakihara, T. Yanagida and H. Noji, *Biophysical Journal*, 2010, **98**, 2014–2023.

32 J. N. Taylor, C.-B. Li, D. R. Cooper, C. F. Landes and T. Komatsuzaki, *Scientific Reports*, 2015, **5**, 9174.

33 M. G. Evans and M. Polanyi, *Trans. Faraday Soc.*, 1935, **31**, 875.

34 H. Eyring, *The Journal of Chemical Physics*, 1935, **445**, 107 – 115.

35 K. A. Dill and S. Bromberg, *Molecular Driving Forces: Statistical thermodynamics in chemistry and biology*, Garland Science, 2010.

36 M. Sugawa, K.-i. Okazaki, M. Kobayashi, T. Matsui, G. Hummer and T. Masaike, *Proceedings of the National Academy of Sciences*, 2016, **113**, E2916.

37 Y. Ito and M. Ikeguchi, *Journal of computational chemistry*, 2010, **31**, 2175–2185.

38 D. Truhlar and A. Kohen, *Proc. Nat. Acad. Sci. USA*, 2001, **98**, 848–851.

39 T.-L. Kuo, S. Garcia-Manyes, J. Li, I. Barel, H. Lu, B. J. Berne, M. Urbakh, J. Klafter and J. M. Fernandez, *Proceedings of the National Academy of Sciences*, 2010, **107**, 11336–11340.

40 T. G. Terentyeva, H. Engelkamp, A. E. Rowan, T. Komatsuzaki, J. Hofkens, C. B. Li and K. Blank, *ACS Nano*, 2012, **6**, 346–

354.
41 T. M. Cover and J. A. Thomas, *Elements of Information Theory*, John Wiley and Sons, 2005, pp. 1–748.
42 E. Yeramian and P. Claverie, *Nature*, 1987, **326**, 169–174.
43 C.-B. Li and T. Komatsuzaki, *Physical Review Letters*, 2013, **111**, 058301.